Accepted Manuscript

Chirality of the trisubstituted nitrogen center – XRD, dynamic NMR, and DFT investigation of 1,2-dihydrobenzo[*e*][1,2,4]triazine derivatives

Piotr Kaszyński, Arkadiusz Kłys, Sławomir Domagała, Krzysztof Woźniak

PII: S0040-4020(17)30507-0

DOI: 10.1016/j.tet.2017.05.032

Reference: TET 28698

To appear in: *Tetrahedron*

Received Date: 16 March 2017

Revised Date: 27 April 2017

Accepted Date: 8 May 2017

Please cite this article as: Kaszyński P, Kłys A, Domagała Sł, Woźniak K, Chirality of the trisubstituted nitrogen center – XRD, dynamic NMR, and DFT investigation of 1,2-dihydrobenzo[*e*][1,2,4]triazine derivatives, *Tetrahedron* (2017), doi: 10.1016/j.tet.2017.05.032.

Tetrahedron March 15, 2017
REVISED: April 26, 2017

Piotr Kaszyński
Centre for Molecular and Macromolecular Studies
Polish Academy of Sciences
Sienkiewicza 112
90363 Łódź, Poland
E-mail: Piotr.kaszynski@mtsu.edu

Chirality of the trisubstituted nitrogen center – XRD, dynamic NMR, and DFT investigation of 1,2-dihydrobenzo[*e*][1,2,4]triazine derivatives

Piotr Kaszyński,*[1,2,3] Arkadiusz Kłys,[2] Sławomir Domagała,[4] and Krzysztof Woźniak[4]

[1] Centre for Molecular and Macromolecular Studies, Polish Academy of Sciences, Sienkiewicza 112, 90363 Łódź, Poland, E-mail: piotrk@cbmm.lodz.pl
[2] Department of Chemistry, University of Łódź, Tamka 12, 91403 Łódź, Poland
[3] Department of Chemistry, Middle Tennessee State University, Murfreesboro, TN 37132, USA
[4] Department of Chemistry, University of Warsaw, Pasteura 5, 02089 Warsaw, Poland

Abstract: Molecular structures of two 1-aryl-2-benzyloxycarbonyl-1,2-dihydrobenzo[*e*][1,2,4]triazines **1** were established by single crystal XRD and compared to those of 4-benzyloxycarbonyl (**2**) and 4-benzyl (**4**) analogues. The structures revealed a highly pyramidalized asymmetric N(1) center stabilized by steric interactions in **1**, but not in **2** and **3**. Activation parameters for enantiomer interconversion were obtained by DNMR methods in C_6D_5Cl: $\Delta H^{\ddagger}$ = 18.1(1) kcal mol^{-1}, $\Delta S^{\ddagger}$ = -0.6(1) cal mol^{-1} K^{-1} for Ar = Ph (**1a**) and $\Delta H^{\ddagger}$ = 18.6(4) kcal mol^{-1}, $\Delta S^{\ddagger}$ = 5.2(6) cal mol^{-1} K^{-1} for Ar = 2-anisyl (**1b**). DFT computational investigation of the origin of the interconversion barrier on model compounds revealed steric destabilization of the inversion TS.

Keywords: chirality, dynamic NMR, heterocyclic chemistry, single crystal XRD, DFT calculations

Graphical abstract

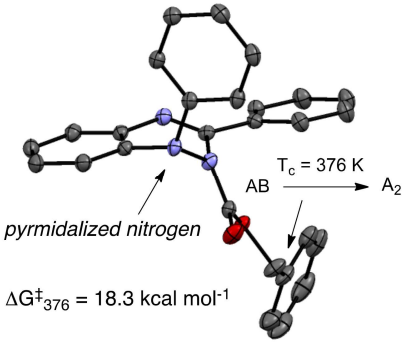

Introduction

A typical tricoordinated nitrogen atom is configurationally labile, and, in contrast to heavier elements such as P and S,[1] its inversion is a low energy process.[2,3] For this reason amine nitrogen atoms are not typically considered stable chirality centers in the absence of any other stereogenic elements in the molecule.[4] Substitution of an amine H atom with a heteroatom possessing a lone pair increases the inversion barrier.[5-10] In particular, substituting with an NH_2 group enhances configurational stability of the nitrogen center,[11] and leads to a complicated conformational behavior of the resulting hydrazines.[12,13] Interaction of the unshared electron pairs results in a gauche conformation or about 90^o torsional angle between the electron pairs in the global minimum, which is in agreement with the "gauche rule"[14] and supported by structural data[15] and computational results.[16,17] Consequently, *N*,*N'*-substituted hydrazines, irrespective of the degree of nitrogen pyramidalization, have axially chiral rotamers. Some, e.g. derivatives of **I** (Figure 1),[18-20] have sizable activation energies to enantiomer interconversion, as evident from observed patterns in the ^{1}H NMR spectra[21,22] and results of dynamic NMR analyses.[18,23-25]

The rotation around the N–N bond is restricted in cyclic hydrazines, and inversion of the pyramidal nitrogen atom becomes the main dynamic process responsible for enantiomer interconversion. The configurational stability of the stereogenic nitrogen center can be enhanced in several ways:[3] a) by increase of pyramidalization of the nitrogen atom through heteroatom substitution, b) by increase of the *s*-character of the unshared pair orbital through confining into a 3-membered ring, c) by increase of rigidity of the cyclic system, d) by planarizing the adjacent N atom, and e) by increase of steric congestion of the substituents. While the first two methods involve changes in the electronic structure of the nitrogen atom in the ground state, the latter three destabilize the inversion TS largely through steric interactions. For instance, activation

energy, $\Delta G^{\ddagger}$, for nitrogen inversion in pyrazolidine (**II**, n = 5, R = Me, Figure 1) is measured at 11.1 kcal mol^{-1}.[5] Contraction of the heterocyclic ring gradually increases the inversion barrier to 16.2 kcal mol^{-1} in diazetidine (**II**, n = 4, R = Me),[26] and to about 27 kcal mol^{-1} in diazirine (**II**, n = 3),[27,28] due to progressively increasing conformational rigidity of the ring and rehybridization of the N atoms. Conformational restriction of pyrazolidine (**II**, n = 5) increases the inversion barrier by about 8 kcal mol^{-1} in 2,3-diazanorbornane **III** (R = Me).[29,30] On the other hand, planarization of the adjacent nitrogen atoms in **II**, n = 5 through the carbamide functionality in **IV** has a modest effect on the configurational stability of the nitrogen center ($\Delta G^{\ddagger}$ = 11.6 kcal mol^{-1}, R = Bn).[31] The preferred orthogonal orientation of the unshared electron pairs prevails also in cyclic *N*,*N*'-diacyl hydrazines (e.g. type **I**, R = COOEt), in which axially chiral enantiomeric conformers are separated by significant activation barriers.[18,29,32]

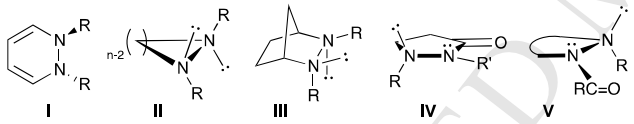

Figure 1. Selected types of cyclic hydrazines.

The search for derivatives with the configurationally stable trisubstituted nitrogen atom as the only source of chirality in a molecule represents an interesting area of organic chemistry. For some monocyclic 1,3,4-oxadiazolidines,[33,34] oxaziridines,[35,36] and 1,3,4-thiadiazolidines[33] activation energies, $\Delta G^{\ddagger}$, exceed 23 kcal mol^{-1}, and enantiomers of several such derivatives have been isolated.[34-36]

Recently, we found evidence of enhanced configurational stability of the pyramidalized nitrogen atom in 1,2-dihydro[1,2,4]triazines, a class of compounds of the general structure **V** (Figure 1) previously not investigated in this context. While working towards

benzo[*e*][1,2,4]triazinyl radicals,[37] we observed an AB diastereotopic pattern of the benzylic hydrogen atoms in the ^{1}H NMR spectra of derivatives **1** (Figure 2).[38] Given the interest in the asymmetric nitrogen atom, this observation prompted us to carry out detailed studies into the nature and origin of the inhibited inversion in **1**. Herein we report molecular and crystal structures for **1a** and **1b**, the first such structures for 1,2-dihydrobenzo[*e*][1,2,4]triazine, and investigate activation parameters for their enantiomer interconversion using variable temperature ^{1}H NMR spectroscopy and DFT computational methods. The molecular structure of **1a** is compared to those of its isomer **2a** and derivative **3a**.

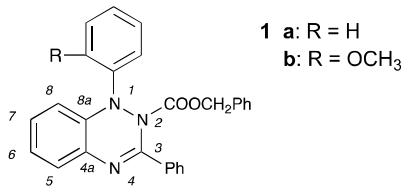

1 **a**: R = H
b: R = OCH_3

Figure 2. The structures of **1a** and **1b** with the numbering scheme for the heterocycle.

Results and Discussion

Synthesis: Compounds **1** were obtained along with their isomers **2** by trapping of the anion **4** with benzyl chloroformate followed by chromatographic separation of the resulting isomers (Scheme 1). Trapping of anion **4a** with benzyl bromide provided an analogous mixture of *N*-benzyl derivatives out of which the 4-benzyl isomer **3a** was isolated in 43% yield. Synthesis and characterization details have been described previously.[38]

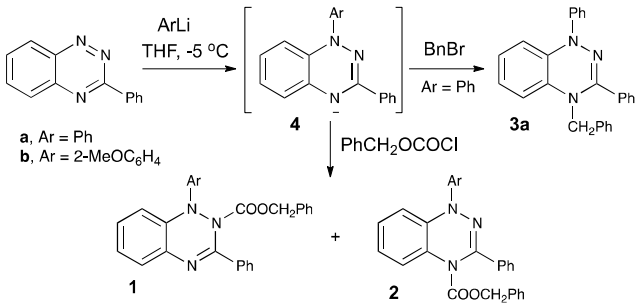

Scheme 1. Synthesis of the 1,2-dihydrobenzo[*e*][1,2,4]triazines **1**, their isomers **2**, and benzyl derivative **3a**.

***Crystal and molecular structures*:** Colorless crystals of **1a** and **2a** were obtained from CH_2Cl_2/cyclohexane, while **1b** and **3a** from petroleum ether/CH_2Cl_2 solutions, and their solid-state structures were determined by low temperature single crystal X-ray diffraction methods. Molecules of **1a**, **2a** and **3a** crystallize in the triclinic *P-1* space group, whereas **1b** crystallizes in the monoclinic $P2_1/c$ space group. Each crystal structure contains one molecule in the asymmetric part of the unit cell. Results are shown in Tables 1 and 2 and in Figures 3-5.

Analysis of the molecular structures of derivatives **1a** and **1b** revealed that the 3-phenylbenzo[*e*][1,2,4]triazine system is approximately planar with the exception of the N(2) atom, which is outside the molecular plane by nearly 0.8 Å (Table 2, Figure 3). This distortion alleviates the unfavorable conjugation of 12 π electrons in the heterocycle core, and also avoids local interactions of unshared electron pairs in the N(1)–N(2) fragment. As a consequence, the substituents on the hydrazine fragment adopt a pseudo *anti* orientation relative to each other, as shown for **1b** in Figure 3. The observed geometry of the N(1)–N(2) fragment, including its bond length of 1.417 Å, are typical for other hydrazide derivatives,[39-42] and the geometry of the 1,2-dihydro[1,2,4]triazine is reminiscent of that found[19,20] for derivatives of type **I** (Figure 1).

Table 1. Crystallographic data for investigated derivatives.[a]

	1a	**1b**	**2a**	**3a**
Empirical formula	$C_{27}H_{21}N_3O_2$ •0.04(H_2O)	$C_{28}H_{23}N_3O_3$	$C_{27}H_{21}N_3O_2$	$C_{26}H_{21}N_3$
Fw	420.28	449.49	419.47	375.46
space group	*P-1*	$P2_1/c$	*P-1*	*P-1*
a, Å	7.6165(3)	18.8954(3)	9.0784(8)	9.5553(5)
b, Å	9.1438(4)	15.8668(3)	10.1684(9)	9.9098(5)
c, Å	16.8190(7)	7.59731(15)	12.7434(11)	11.6678(5)
α, deg	91.840(3)	90	78.137(3)	94.551(4)
β, deg	102.242(4)	94.2861(16)	85.341(3)	98.953(4)
γ, deg	108.813(4)	90	63.899(3)	115.869(5)
V, $Å^3$	1077.14(8)	2271.37(7)	1033.80(16)	968.45(9)
Z	2	4	2	2
ρ (calcd), g/cm^3	1.296	1.314	1.348	1.288
μ, mm^{-1}	0.083	0.087	0.087	0.077
R_{int}	0.0396	0.0720	0.0258	0.0490
R^b ($I > 2\sigma(I)$)	0.0495	0.0489	0.0413	0.0562
$R_w{}^c$ ($I > 2\sigma(I)$)	0.1243	0.1221	0.1133	0.1400
R (all data)	0.0673	0.0650	0.0446	0.0806
R_w (all data)	0.1384	0.1322	0.1172	0.1581
goodness of fit on F^2	1.037	1.029	1.023	1.050

[a] Temperature 100 K, λ = 0.71073 Å; [b] $R = \sum||Fo| - |Fc||/\sum|Fo|$. [c] $R_w = [\sum[w(Fo^2 - Fc^2)^2]/\sum[w(Fo^2)^2]]^{1/2}$

Table 2. Selected interatomic distances (Å) and angles (^{o}) for investigated derivatives. [a]

	1a	**1b**	**2a**	**3a**
N(1)–N(2)	1.417(1)	1.417(1)	1.4052(9)	1.428(2)
N(2)–C(3)	1.426(1)	1.428(1)	1.282(1)	1.290(1)
C(3)–N(4)	1.289(2)	1.288(1)	1.4260(9)	1.399(1)
N(1)–C_{Ph}	1.439(2)	1.437(1)	1.440(1)	1.436(2)
N–CO	1.390(1)	1.391(1)	1.3835(9)	–
C(3)–C_{Ph}	1.475(2)	1.475(1)	1.480(1)	1.485(2)
C=O	1.202(1)	1.202(1)	1.211(1)	–
N(1) pyramid [b]	0.411	0.380	0.349	0.344
N(2) pyramid [b]	0.173	0.193	–	–
N(4) pyramid [b]	–	–	0.101	0.140
N(2)···Benzene [c]	0.793	0.769	0.755	0.675
C_{Ph}–N(1)–N(2)–CO	126.8	125.8	–	–
COO···NR_2 [d]	25.4	23.1	15.0	–
N(1)Ar···Benzene [e]	87.4	79.7	82.8	80.1
C(3)Ph···Benzene [f]	5.1	5.2	45.3	47.2
Ring puckering [g]	–	–	36.2	37.6

[a] Numbering according to the chemical structures. [b] Distance (in Å) of the N atom from the plane defined by its three substituents. [c] Distance (in Å) of the N atom from the plane defined the benzene ring of the heterocycle. [d] Angle between planes defined by the three atoms of each fragment. [e] Angle between planes of the phenyl ring at the N(1) and the benzene ring of the heterocycle. [f] Angle between planes of the phenyl ring at the C(3) and the benzene ring of the heterocycle. [g] Angle between N(1)–C(8a)–C(4a)-N(4) and N(1)–N(2)–C(3)-N(4) planes.

The carbonyl group in **1** is partially conjugated with the adjacent nitrogen atom N(2): the nitrogen center is significantly planarized, and the planes defined by the COO and C(3)N(2)N(1) fragments form an angle of about 25^{o} (Table 2).

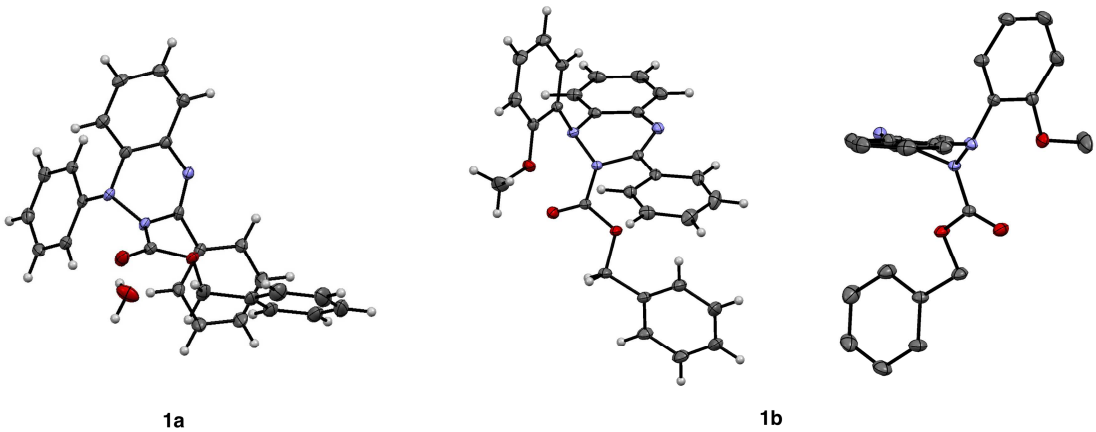

Figure 3. Thermal ellipsoid diagrams drawn at 50% probability for **1a** (shown with crystallization H_2O) and two views of **1b** (with and without H atoms for clarity). Oxygen atoms are marked in red and nitrogen in blue. Pertinent molecular dimensions are listed in Table 2.

In contrast, high degree of pyramidalization of the N(1) atom and nearly orthogonal orientation of the attached Ph ring prevent effective conjugation with the adjacent aromatic systems (Figure 3). Thus, as a consequence of the pyramidalization and steric congestion, the N(1) nitrogen atom can be considered as a stereogenic center of enhanced configurational stability responsible for the observed diastereotopic splitting of the benzylic hydrogen atoms in the ^{1}H NMR spectrum of **1**. In addition, it possesses a lone pair with a significant *s*-character pointing to the center of the chiral cavity formed by three benzene rings and the carbonyl group as shown in Figure 4 for **1b**.

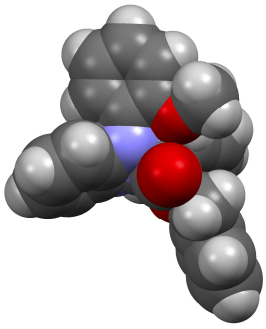

Figure 4. A space-filling model of the experimental structure of **1b** showing the N(1) nitrogen atom.

A comparison of the **1a** and **2a** isomers is instructive. In the 4-COOBn isomer **2a** and also in the 4-benzyl derivative **3a** the [1,2,4]triazine ring adopts a chevron or "open book" conformation, characteristic for 8-π electron six-membered heterocyclic 1,4-dienes,[43] with a puckering angle of about 37^o (Table 2). Less steric congestion around the amide bond, allows for a more efficient overlap between the π_{CO}* orbital and the lone pair n_N in **2a** than in the **1a** isomer. This is evident from the closest to parallel COO and NR_2 planes, most planarized nitrogen atom and, as a consequence of most effective electron density transfer from N to CO, the shortest N–CO bond and the longest C=O distance in the investigated series (Table 2). The Ph ring at the N(1) position bisects the puckering angle (the Ph···N(2)-C(3)-C(4a)-C(8a) interplanar angle is 78.5^o for **2a** and 63^o for **3a**), while the Ph ring at the C(3) position adopts a staggered conformation with respect to the adjacent C(3)=N(2) bond with the torsion angle of 43^o and 49^o for **2a** and **3a**, respectively (Figure 5). The N(1) is still significantly pyramidalized in both compounds, but the planar, dicoordinated N(2) center does not inhibit interconversion of chiral conformers. Structures of **2a** and **3a** complement two other structurally characterized derivatives of 1,4-dhydrobenzo[*e*][1,2,4]triazine.[44,45]

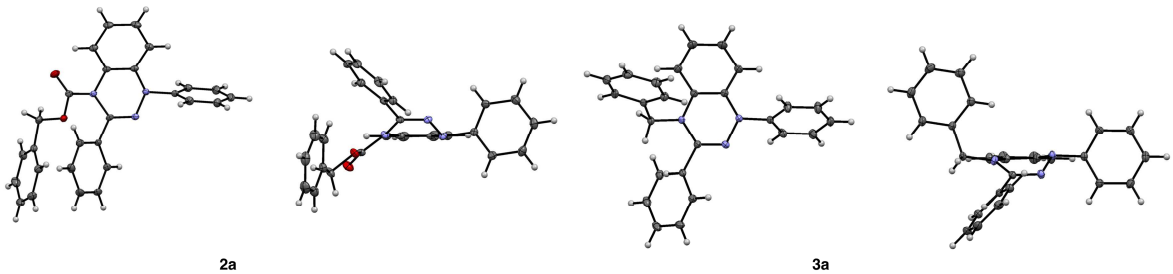

Figure 5. Thermal ellipsoid diagrams drawn at 50% probability for two views of **2a** and **3a**. Pertinent molecular dimensions are listed in Table 2.

In three derivatives, **1a**, **2a**, and **3a**, the unit cell contains two molecules related by inversion symmetry, while the unit cell of the methoxy derivative **1b** contains four molecules. In addition, the unit cell of **1a** contains two molecules of water of crystallization modelled with 4% occupancy. Therefore, statistically every 25-th unit cell is occupied by two water molecules.

Significant intermolecular interactions have been found in the crystal structures of **1b**, **2a**, and **3a**. For instance, in **1b** the C=O$^{\cdots}$ CH_3O contact is 0.35 Å shorter than the sum of van der Waals (VDW) radii of O and C atoms resulting in a chain structure. Similar $CH_2^{\cdots}$O=C interactions in **2a** lead to a dimeric structure. In **3a**, the benzylic HCH$^{\cdots}$HCH distance between neighboring molecules is 0.229 Å inside the H$^{\cdots}$H VDW separation, which also results in a dimeric structure.

***Dynamic NMR measurements*:** Ambient temperature ^{1}H NMR spectra of **1a** and **1b** in C_6D_5Cl show the benzylic CH_2 protons as the AB pattern with the $^2J_{HH}$ = 12.5 Hz for **1a** and the $^2J_{HH}$ = 12.6 Hz for **1b**, indicating their magnetic nonequivalence (Figure 6). With increasing temperature the rate of inversion also increases and the signals coalesce at T_c = 376 and 341 K for **1a** and **1b**, respectively. The calculated free energy of activation, $\Delta G_{Tc}^{\ddagger}$, for the process is 18.3 and 16.8 kcal mol^{-1} for **1a** and **1b**, respectively.[46]

Complete line shape analysis performed for a series of spectra shown in Figure 6 followed by standard Arrhenius analysis of the resulting exchange rates k_r *vs* temperature (Figure 7) gave the activation parameters, $\Delta H^{\ddagger}$ and $\Delta S^{\ddagger}$, listed in Table 3.

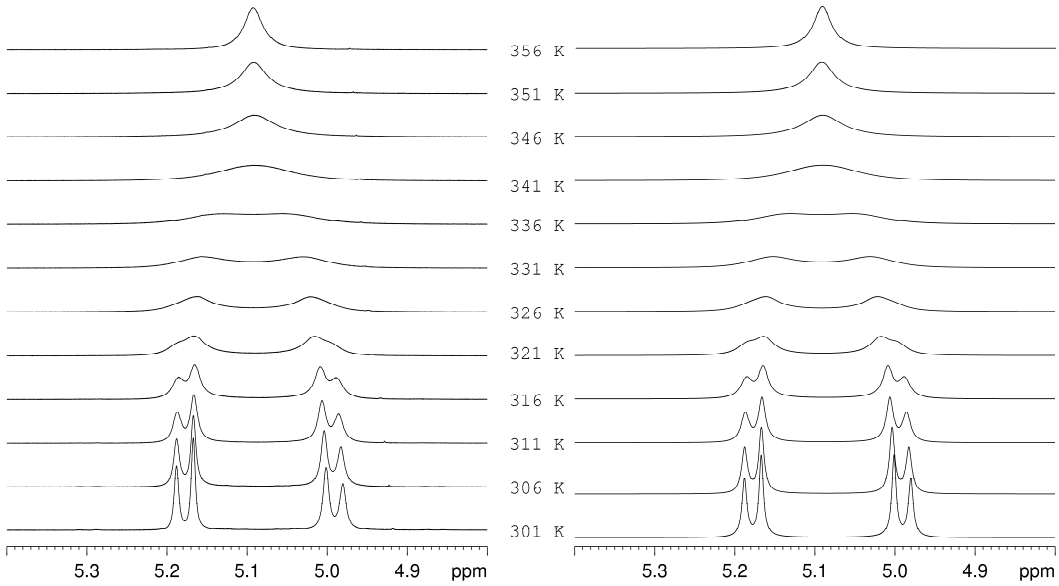

Figure 6. Stacked ^{1}H NMR spectra of **1b** in C_6D_5Cl: experimental (left) and simulated (right).

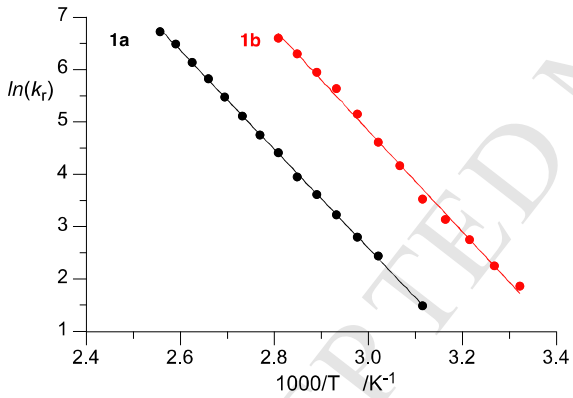

Figure 7. Arrhenius plot of exchange rate k_r *vs* T for **1a** and **1b** obtained from complete line shape analysis of spectra in Figure 6. Fitting values are in Table 3. Correlation parameter r^2 > 0.996.

Results show that the enthalpy of activation, $\Delta H^{\ddagger}$, to inversion is about 18 kcal mol^{-1} for both derivatives with a slightly higher value for the methoxy derivative **1b**. The determined entropy of activation, $\Delta S^{\ddagger}$, is weakly negative for **1a** indicating a more organized TS relative to the GS, in accordance with the theoretical model (*vide infra*). In contrast, the positive value of $\Delta S^{\ddagger}$ obtained for the methoxy derivative **1b** indicates a less organized TS, which may suggest

solvation effects. As a consequence of the positive $\Delta S^{\ddagger}$ value, the MeO derivative **1b** is more configurationally labile than **1a** in spite of higher $\Delta H^{\ddagger}$.

Table 3. Results of analysis of variable temperature ^{1}H NMR spectroscopy measurements for **1a** and **1b** in C_6D_5Cl. [a]

compound	Activation parameters [b]		Thermodynamic parameters at 25 °C			T_c	$\Delta G^{\ddagger}_{Tc}$ at T_f /kcal mol^{-1}	
	*ln*A	E_a /kcal mol^{-1}	$\Delta H^{\ddagger}$ /kcal mol^{-1}	$\Delta S^{\ddagger}$ /cal mol^{-1} K^{-1}	$\Delta G^{\ddagger}_{298}$ /kcal mol^{-1}	/K	From Arrhenius	From T_c
1a	30.87±0.1	18.73±0.1	18.1±0.1	-0.6±0.1	18.3±0.1	376	18.4±0.1	18.3±0.1
1b	33.76±0.6	19.2±0.4	18.6±0.4	5.2±0.6	17.0±0.4	341	16.8±0.4	16.8±0.1

[a] Variable temperature NMR spectroscopy data shown in Figure 5. [b] From fitting kinetic data in Figure 6.

***Computational analysis*:** For a better understanding of factors responsible for configurational stability of **1** and to the support NMR spectroscopy results, DFT calculations were conducted at the B3LYP/6-31G(2d,p) level of theory for model derivatives **5**–**10** (Figure 8).

Analysis of the simplest system, 1-phenyl-1,2-dihydro[1,2,4]triazine (**5**), revealed a twisted structure similar to that observed in **1a** and 1,2-dihydropyrazines of type I: the N(1) and N(2) atoms are significantly displaced from the ring plane and the 1-phenyl substituent is bent away from the ring (angle α N(4)$\cdots$N(1)-C_{Ph} = 133^o). The interconversion to the opposite conformational enantiomer involves inversion of the ring and both nitrogen atoms, as shown in Figure 9 for **5**: the N(1) center essentially planarizes (τ changes from 0.141 Å in **5** to 0.077 Å in **5-TS**), while pyramidalization of the N(2) center is little changed in **5-TS**. The dihedral angle θ (H–N(2)–N(1)-C_{Ph}, Figure 8) deceases from 119.3^o to 8.3^o in **5-TS** (Table 4) and the calculated barrier to inversion in **5**, $\Delta H^{\ddagger}$, is only 5.02 kcal mol^{-1}.

Substitution of the carboxyl group at the N(2) position in derivative **6** increases the barrier to 12.76 kcal mol^{-1}. In contrast, fusing a benzene ring at the *e* edge results in reduction of the barrier by about 2 kcal mol^{-1} in **8** when compared to **5**. Further increase of the inversion barrier in **5** is achieved by placing a Ph substituent at the C(3) position in **7**. The same trend repeats for the 1,2-dihydrobenzo[*e*][1,2,4]triazine series **8**–**10** for which the activation enthalpies are about 2 kcal mol^{-1} lower than those in the monocyclic analogous **5**–**7** (Figure 8).

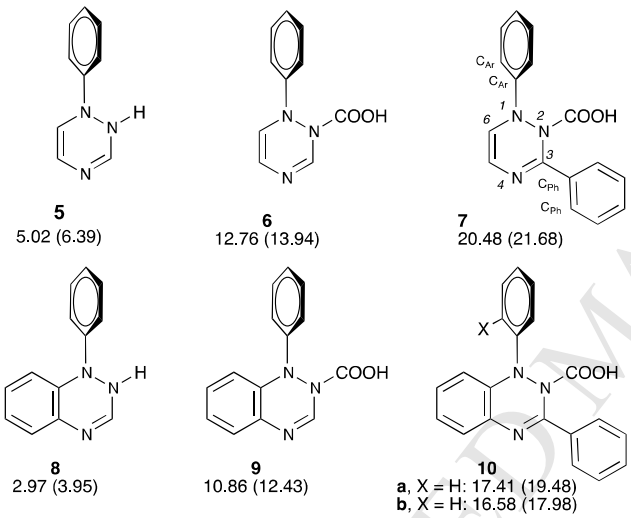

Figure 8. The structures of compounds investigated by the B3LYP/6-31G(2d,p) method and activation parameters for inversion ($\Delta H^{\ddagger}$ and in parentheses $\Delta G^{\ddagger}_{298}$, kcal mol^{-1}). Numbering in **7** defines structural elements in all derivatives **5**-**10** used in Table 4.

Analysis of the geometry of the ground and transition state structures for the monocyclic derivatives revealed that introduction of the COOH group, or fusing a benzene ring to **5** changes the orientation of the N(1) benzene ring in the TS from nearly parallel (ϕ = 13.8^{o}) to almost perpendicular to the heterocyclic ring (ϕ = 123.3^{o} in **6** and ϕ = 87.0^{o} in **8**; Table 4). Steric strain of the substituent is also apparent in the GS: the angle N(4)$\cdots$N(1)-C_{Ph} decreases from α = 137.9 in **5** by 11.5^{o} in **6** and by 17.4^{o} in the benzo-fused derivative **8**. While the COOH group can avoid

steric interactions with the *ortho* hydrogen atoms of the N(1) phenyl group by twisting ($\psi_{C(3)–N(2)-C=O}$ = 167^o), the fused benzene ring cannot. This leads to destabilization of the GS in **8** and decrease in activation energy by about 2 kcal mol^{-1} relative to **5** (Figure 8). This trend is observed in all three dihydrobenzo[*e*][1,2,4]triazines.

Substitution of a Ph group at the C(3) position leads to steric congestion in **7-TS**: the passing of the heterocyclic ring plane by the COOH group during the inversion process is hindered by the Ph group (nearly co-planar in the GS; $\omega_{N(4)–C(3)-CPh-CPh}$ = 13.9^o) at the C(3) position. As a consequence, both the COOH and C(3)–Ph groups are twisted in the TS from the preferred parallel orientation by about $\Delta\psi$ = 20^o and $\Delta\omega$ = 35 ^{o}, respectively, which, along with steric interactions, contributes to the increase in the activation enthalpy (Figure 8). Similar geometrical and thermodynamic effects are observed in **10a**, when compared to **9**. Interestingly, the relative orientation of the N(1) and N(2) substituents also changes, and the dihedral angle $\theta_{X–N(2)–N(1)-CPh}$ increases upon substitution of the Ph at the C(3) position, further demonstrating steric congestion.

Finally, substitution of the MeO group at the *ortho* position of the N(1)–Ph ring leads to destabilization of the GS in **10b** due to steric interactions, and the calculated enthalpy of activation, $\Delta H^{‡}$, for the inversion process is lower by about 0.8 kcal mol^{-1} relative to the **10a** analogue. Overall the calculated free energies of activation, $\Delta G^{‡}_{298}$, for the model derivatives **10a** and **10b** are about 1 kcal mol^{-1} higher than those obtained experimentally for **1a** and **1b** (Table 3). Nevertheless, these results represent a reasonably good agreement between theory and experiment, considering gas phase calculations of simplified models.

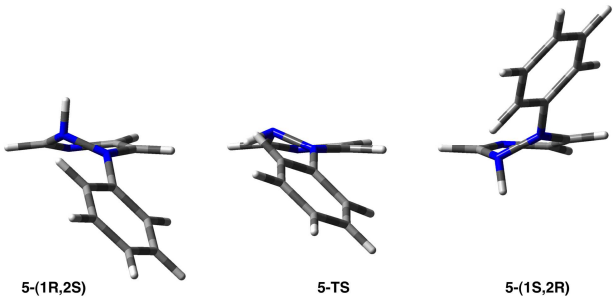

Figure 9. DFT optimized geometry of two enantiomeric GS and inversion TS for **5**. The connection of the three structures was verified with IRC calculations.

Table 4. Selected structural parameters for ground states and inversion transition states of models **5**–**10**. [a]

compound		α N(4)···N(1)-C_{Ar}	ϕ C(6)–N(1)-C_{Ar}-C_{Ar}	θ X–N(2)-N(1)-C_{Ar}	ψ C(3)–N(2)-C_X=O	ω N(4)–C(3)-C_{Ph}-C_{Ph}
5	GS	137.9	4.6	119.5	–	–
	TS	149.3	13.8	8.3	–	–
6	GS	126.4	12.0	100.8	167.4	–
	TS	166.6	123.3	17.7	169.0	–
7	GS	135.5	15.3	106.1	161.1	13.9
	TS	137.0	106.0	54.9	142.5	49.1
8	GS	120.5	9.0	114.4	–	–
	TS	148.1	87.0	74.6	–	–
9	GS	115.3	11.8	100.8	173.8	–
	TS	174.6	64.9	8.3	169.0	–
10a	GS	124.9	13.8	109.8	167.6	20.0
	TS	159.1	67.2	31.7	132.5	42.0

[a] For definition of the structural elements see Figure 8.

Geometry optimization of **1a** and **1b** at the same level of theory reproduced closely the experimental structures with essentially the same conformational features. Attempts at location of the transition state geometries for the inversion process in **1a** and **1b** were unsuccessful. Due to significant molecular flexibility, only rotational transition states of the ester group were found using the QST3 algorithm.

Conclusions

Substituted 1,2-dihydrobenzo[*e*][1,2,4]triazine derivatives possessing a chiral nitrogen atom as the key chirality center have been structurally characterized for the first time. The N(1) nitrogen atom of the [1,2,4]triazine ring is significantly pyramidalized mainly due to interactions with the adjacent N(2) atom. The configurational stability of this stereocenter is further enhanced by the presence of the neighboring substituents, and the enthalpy of activation $\Delta H^{\ddagger}$ of the inversion process is about 18 kcal mol^{-1}. Computational analysis of model compounds indicates that the observed barrier to inversion results mainly from steric interaction of the substituents. Thus, substitution of the [1,2,4]triazine ring in positions 2 and 3 appears to destabilize the inversion TS, while the fused benzene ring and the MeO group on the 1-Ph ring destabilize the GS, hence lower the barrier to inversion.

The present derivatives **1** are still too labile for separation into enantiomers. Results suggest however, that 1,2,3-trisubstituted 1,2-dihydro[1,2,4]triazines with a bulky acyl group (e.g. pivaloyl) at the N(2) position may sufficiently stabilize the configuration of the N(1) center and permit isolation of enantiomers.

Computational Details

Quantum-mechanical calculations were carried out using the Gaussian 09 suite of programs.[47] Geometry optimizations were undertaken at the B3LYP/6-31G(2d,p) level of theory using default convergence limits. Transition state structures were located using the QST3 method, for which ground state input structures were obtained by full geometry optimizations of the both enantiomeric conformers, while the approximate transition state structures were generated using relaxed scans of the PES with varied X–N(2)–N(1)–C_{Ph} dihedral angle. Vibrational frequencies

were used to characterize the nature of the stationary points and to obtain thermodynamic parameters. Zero-point energy (ZPE) corrections were scaled by 0.9806.[48] Reaction path was followed for derivative **5** and **6** from the inversion transition state structure in both directions using the keyword "IRC=(RCFC, LQA, recorrect=never, recalc=-5, maxpoint=300, tight)" and specifying "forward" or "reverse".

Experimental Section

Synthesis. Compounds **1**–**3** were obtained as described before.[38]

X-Ray data collection. Single-crystal X-ray measurements for **1a**, **1b**, **2a**, and **3a** were performed with a Supernova diffractometer equipped with an Eos detector (**1a**, **3a**), Supernova Dual diffractometer with an Atlas detector (**1b**) and a Bruker Apex-II CCD diffractometer (**2a**). All measurements were conducted at 100 K using the Mo Kα radiation. The crystals were positioned at 74 and 50 mm from the Atlas and Eos/Apex-II detector, respectively. A total number of 1020, 1394, 2925 and 799 frames were collected at 1° intervals with a counting time of 30s, 50s, 15s and 35s for **1a**, **1b**, **2a** and **3a**, respectively. The data were corrected for Lorentzian and polarization effects. Data reduction and analysis were carried out with the Crysalis program (Agilent, CrysAlis PRO, Agilent Technologies, Yarnton, England, 2012). The structures were solved by direct methods and refined using SHELXL-97[49] within the Olex2 program.[50] The refinement was based on F^2 for all reflections except those with very negative F^2. Weighted R factors (wR) and all goodness-of-fit (GooF) values are based on F^2. Conventional R factors are based on F with F set to zero for negative F^2. The $F_o^2 > 2\sigma(Fo^2)$ criterion was used only for calculating the R factors and it is not relevant to the choice of reflections for the refinement. The R factors based on F^2 are about twice as large as those based on F. Scattering factors were

taken from the International Tables for Crystallography.[51] All hydrogen atoms were placed in idealized positions. A small amount of water ~4% per one molecule of main moiety is present in the case of **1a**. The structures have been deposited at CCDC (1522807-1522810).

Temperature-dependent ^{1}H NMR spectroscopy and data analysis. Variable temperature ^{1}H NMR spectra of **1a** and **1b** were recorded at 600 MHz in C_6D_5Cl at several temperatures typically every 5 K (with 15 min of stabilization). The geminal coupling constant $^2J_{HH}$ for each compound was dßetermined at the lowest temperature (301 K, $^2J_{HH}$ = 12.5 Hz for **1a** and $^2J_{HH}$ = 12.6 Hz for **1b**) and assumed to be the same at all investigated temperatures.

Experimental activation parameters. To establish activation parameters for the inversion process with the Arrhenius method, the exchange rate, k_r, was established by complete line shape analysis using the DNMR utility in TopSpin 2.1 software package.[52] Thus, sections of the experimental spectra for the benzylic CH_2 group (4.8 – 5.3 ppm) were simulated by variation of two parameters: line broadening (L_b) and rate of exchange (k_r), to obtain correlation >96%. Alternatively, $\Delta G^{\ddagger}$ value for each derivative was calculated from the coalescence temperature, T_c. The separation $\Delta\nu$ between signals of diastereotopic hydrogen atoms was measured at the lowest temperature (301 K), and the transmission coefficient κ was assumed to be 0.5, since the reaction involves a degenerate process.[53] Details are provided in the ESI.

Acknowledgements

Support for this project was provided by the National Science Center (2014/13/B/ST5/04525). The authors thank Dr. Emilia Obijalska for preparation of suitable crystals for XRD analysis.

References

(1) Lambert, J. B. *Top. Stereochem.* **1971**, *6*, 19-105.

(2) Swalen, J. D.; Ibers, J. A. *J. Chem. Phys.* **1962**, *36*, 1914-1918.

(3) Lehn, J. M. *Top. Curr. Chem.* **1970**, *15*, 311-377, and references therein.

(4) Steric congestion significantly hinders inversion of the nitrogen atom in *N*-substituted 1,2-dihydrobenzo[*h*]quinolones ($\Delta H^{\ddagger}$ = 22 kcal mol^{-1}, $\Delta S^{\ddagger}$ = 9.6 cal $K^{-1}mol^{-1}$, Ea = 23 kcal mol^{-1}. Speckamp, W. N.; Pandit, U. K.; Korver, P. K.; van der Haak, P. J.; Huisman, H. O. *Tetrahedron* **1966**, *22*, 2413-2427.

(5) Lehn, J. M.; Wagner, J. *Tetrahedron* **1970**, *26*, 4227-4240.

(6) Kostyanovsky, R. G.; Rudchenko, V. F.; Shtamburg, V. G.; Chervin, I. I.; Nasibov, S. S. *Tetrahedron* **1981**, *37*, 4245-4254.

(7) Shustov, G. V.; Kadorkina, G. K.; Kostyanovsky, R. G.; Rauk, A. *J. Am. Chem. Soc.* **1988**, *110*, 1719–1726.

(8) Shustov, G. V.; Tavakalyan, N. B.; Kostyanovsky, R. G. *Tetrahedron* **1985**, *41*, 575-584.

(9) Prosyanik, A. V.; Mishchenko, A. I.; Zelenskaya, O. V.; Forni, A.; Moretti, I.; Torre, G.; Brükner, S.; Malpezzi, L.; Kostyanovsky, V. R.; Kostyanovsky, R. G. *Russ. Chem. Bull.* **1998**, *47*, 1359–1364.

(10) Rudchenko, V. F. *Chem. Rev.* **1993**, *93*, 725–739.

(11) Hamada, Y.; Hirakawa, A. Y.; Tamagake, K.; Tsuboi, M. *J. Mol. Spect.* **1970**, *35*, 420-435.

(12) Shvo, Y. In *The chemistry of the hydrazo, azo and azoxy groups* Patai, S., Ed.; Wiley&Sons: New York, 1975; Vol. 2, p 1017-1095.

(13) Jones, R. A. Y.; Katritzky, A. R.; Record, K. A. F.; Scattergood, R. *J. Chem. Soc. Perkin Trans 2* **1974**, 406-415.

(14) "When electron pairs or polar bonds are placed or generated on adjacent pyramidal atoms, syn or anti periplanar orientation is energetically disfavored with respect to a structure which contains the maximum number of gauche interctions", Wolfe, S. *Acc. Chem. Res.* **1972**, *5*, 102-111.

(15) For example: (a) Wang, X.-Y.; Narita, A.; Feng, X.; Müllen, K. *J. Am. Chem. Soc.* **2015**, 137, 7668–7671. (b) Ottersen, T. *Acta Chem. Scand., Series A* **1978**, *32*, 127–131. (c) Ray, J. K.; Mahato, T. K.; Chinnakali, K.; Fun, H.-K. *Acta Crystallogr. Sect. C* **1997**, *53*, 1621-1622. (d)

Garric, J.; Léger, J.-M.; Grelard, A.; Ohkita, M.; Huc, I. *Tetrahedron Lett.* **2003**, *44*, 1421–1424. (e) Lau, Y.-F.; Chan, C.-M.; Zhou, Z.; Yu, W.-Y. *Org. Biomol. Chem.* **2016**, *14*, 6821-6825. (f) Dietrich, M.; Heinze, J.; Krieger, C.; Neugebauer, F. A. *J. Am. Chem. Soc.* **1996**, *118*, 5020–5030.

(16) Schlegel, H. B.; Skancke, A. *J. Am. Chem. Soc.* **1993**, *115*, 7465-7471.

(17) Song, J.-W.; Lee, H.-J.; Choi, Y.-S.; Yoon, C.-J. *J. Phys. Chem. A* **2006**, *110*, 2065-2071.

(18) Anderson, J. E.; Lehn, J. M. *Tetrahedron* **1968**, *24*, 137-149.

(19) Kaftory, M. *J. Chem. Soc., Perkin Trans 2* **1989**, 1887-1891.

(20) Dietrich, M.; Heinze, J.; Krieger, C.; Neugebauer, F. A. *J. Am. Chem. Soc.* **1996**, *118*, 5020–5030.

(21) Rasmussen, L. K. *J. Org. Chem.* **2006**, *71*, 3627-3629.

(22) Ball, C. J.; Gilmore, J.; Willis, M. C. *Angew. Chem. Int. Ed.* **2012**, *51*, 5718-5722.

(23) Fletcher, J. R.; Sutherland, I. O. *Chem. Commun.* **1969**, 706-708.

(24) Fletcher, J. R.; Sutherland, I. O. *Chem. Commun.* **1970**, 687-688.

(25) Bishop, G. J.; Price, B. J.; Sutherland, I. O. *Chem. Commun.* **1967**, 672-674.

(26) Hall, J. H.; Bigard, W. S. *J. Org. Chem.* **1978**, *43*, 2785-2788.

(27) Mannschreck, A.; Seitz, W. *Angew. Chem. Int. Ed.* **1968**, *8*, 212-213.

(28) Trapp, O.; Schurig, V.; Kostyanovsky, R. G. *Chem. Eur. J.* **2004**, *10*, 951–957.

(29) Anderson, J. E.; Lehn, J. M. *Tetrahedron* **1968**, *24*, 123-135.

(30) Allred, E. L.; Anderson, C. L.; Miller, R. L.; Johnson, A. L. *Tetrahedron Lett.* **1967**, 525-531.

(31) Elguero, J.; Marzin, C.; Tizané, D. *Org. Magn. Res.* **1969**, *1*, 249-275.

(32) Lenev, D. A.; Lyssenko, K. A.; Golovanov, D. G.; Weingart, O.; Buß, V.; Kostyanovsky, R. G. *Tetrahedron: Asymmetry* **2004**, *15*, 537–543.

(33) Kostyanovsky, R. G.; Rademacher, P.; Elnatanov, Y. I.; Kadorkina, G. K.; Nikiforov, G. A.; Chervin, I. I.; Usachev, S. V.; Kostyanovsky, V. R. *Russ. Chem. Bull.* **1997**, *46*, 1291–1299.

(34) Kostyanovsky, R. G.; Kadorkina, G. K.; Kostyanovsky, V. R.; Schurig, V.; Trapp, O. *Angew. Chem. Int. Ed.* **2000**, *39*, 2938-2940.

(35) Bjørgo, J.; Boyd, D. R. *J. Chem. Soc., Perkin Trans. 2* **1973**, 1575-1577

(36) Montanari, F.; Moretti, I.; Torre, G. *Chem. Commun.* **1969**, 1086-1087.

(37) For example: (a) Blatter, H. M.; Lukaszewski, H. *Tetrahedron Lett.* **1968**, *9*, 2701-2705. (b) Neugebauer, F. A.; Umminger, I. *Chem. Ber.* **1980**, *113*, 1205-1225. (c) Constantinides, C. P.; Koutentis, P. A.; Loizou, G. *Org. Biomol. Chem.* **2011**, *9*, 3122-3125. (d) Constantinides, C. P.; Berezin, A. A.; Zissimou, G. A.; Manoli, M.; Leitus, G. M.; Bendikov, M.; Probert, M. R.; Rawson, J. M.; Koutentis, P. A. *J. Am. Chem. Soc.* **2014**, *136*, 11906−11909. (e) Berezin, A. A.; Zissimou, G.; Constantinides, C. P.; Beldjoudi, Y.; Rawson, J. M.; Koutentis, P. A. *J. Org. Chem.* **2014**, *79*, 314-327. (f) Bodzioch, A.; Zheng, M.; Kaszyński, P.; Utecht, G. *J. Org. Chem.* **2014**, *79*, 7294-7310. (g) Zheng, Y.; Miao, M.-s.; Kemei, M. C.; Ram Seshadri, R.; Wudl, F. *Isr. J. Chem.* **2014**, *54*, 774–778.

(38) Constantinides, C. P.; Obijalska, E.; Kaszynski, P. *Org. Lett.* **2016**, *18*, 916-919.

(39) Garric, J.; Léger, J.-M.; Grelard, A.; Ohkita, M.; Huc, I. *Tetrahedron Lett.* **2003**, *44*, 1421–1424.

(40) Lau, Y.-F.; Chan, C.-M.; Zhou, Z.; Yu, W.-Y. *Org. Biomol. Chem.* **2016**, *14*, 6821-6825.

(41) Yeh, M.-Y.; Huang, C.-Y.; Ueng, C.-H.; Wang, Y. *Acta Crystallogr. Sect. C* **1994**, *50*, 1781-1784.

(42) Billert, T.; Beckert, R.; Fehling, P.; Döring, M.; Brandenburg, J.; Görls, H.; Langer, P. *J. Heterocycl. Chem.* **1999**, *36*, 627-633.

(43) For example: (a) Farrar, J. M.; Patel, M. K.; Kaszynski, P.; Young, V. G. Jr. *J. Org. Chem.* **2000**, *65*, 931-940. (b) Butler, R. N.; Evans, A. M.; McNeela, E. M.; O'Halloran, G. A.; O'Shea, P. D.; Cunningham, D.; McArdle, P. *J. Chem. Soc., Perkin Trans. 1* **1990**, 2527-2536. (c) Daley, S. T. A. K.; Rees, C. W.; Williams, D. J. *J. Chem. Soc., Chem. Commun.* **1984**, 57-59. (d) Sundermeyer, J.; Roesky, H. W.; Noltemeyer, M. *Angew. Chem. Int. Ed.* **1989**, *28*, 609-610.

(44) Morgan, I. S.; Mansikkamäki, A.; Zissimou, G. A.; Koutentis, P. A.; Rouzières, M.; Clérac, R.; Tuononen, H. M. *Chem. Eur. J.* **2015**, *21*, 15843–15853

(45) Areephong, J.; Mattson, K. M.; Treat, N. J.; Poelma, S. O.; Kramer, J. W.; Sprafke, H. A.; Latimer, A. A.; Read de Alaniz, J.; Hawker, C. J. *Polym. Chem.* **2016**, *7*, 370-374.

(46) For more details see the SI.

(47) Gaussian 09, Revision A.02, M. J. Frisch, G. W. Trucks, H. B. Schlegel, G. E. Scuseria, M. A. Robb, J. R. Cheeseman, G. Scalmani, V. Barone, B. Mennucci, G. A. Petersson, H. Nakatsuji, M. Caricato, X. Li, H. P. Hratchian, A. F. Izmaylov, J. Bloino, G. Zheng, J. L. Sonnenberg, M. Hada, M. Ehara, K. Toyota, R. Fukuda, J. Hasegawa, M. Ishida, T. Nakajima, Y. Honda, O.

Kitao, H. Nakai, T. Vreven, J. A. Montgomery, Jr., J. E. Peralta, F. Ogliaro, M. Bearpark, J. J. Heyd, E. Brothers, K. N. Kudin, V. N. Staroverov, R. Kobayashi, J. Normand, K. Raghavachari, A. Rendell, J. C. Burant, S. S. Iyengar, J. Tomasi, M. Cossi, N. Rega, J. M. Millam, M. Klene, J. E. Knox, J. B. Cross, V. Bakken, C. Adamo, J. Jaramillo, R. Gomperts, R. E. Stratmann, O. Yazyev, A. J. Austin, R. Cammi, C. Pomelli, J. W. Ochterski, R. L. Martin, K. Morokuma, V. G. Zakrzewski, G. A. Voth, P. Salvador, J. J. Dannenberg, S. Dapprich, A. D. Daniels, O. Farkas, J. B. Foresman, J. V. Ortiz, J. Cioslowski, and D. J. Fox, Gaussian, Inc., Wallingford CT, 2009.

(48) Scott, A. P.; Radom, L. *J. Phys. Chem.* **1996**, *100*, 16502-16513.

(49) Sheldrick, G. M. *Acta Crystallogr. Section A* **2008**, *64*, 112–122.

(50) Dolomanov, O. V.; Bourhis, L. J.; Gildea, R. J.; Howard, J. A. K.; Puschmann, H. *J. Appl. Crystallogr.* **2009**, *42*, 339-341.

(51) International Tables for Crystallography; Schmueli, U., Ed.; Springer: New York, 2006.

(52) TopSpin, Version 2.1 (March 5, 2009), The Next Generation in NMR Software, 2009 Bruker BioSpin.

(53) (a) Jackman, L. M. In Organic Molecules in Dynamic NMR Spectroscopy; Jackman, L. M., Cotton, F. A., Eds.; Academic: New York, NY, 1975; pp 203-217; (b) Sandström, J. Dynamic NMR Spectroscopy; Academic: London, 1982; pp 93-123 and 151-176; (c) Oki, M. Applications of Dynamic NMR Spectroscopy to Organic Chemistry. Methods in Stereochemical Analysis; VCH: Weinheim, 1985; Vol. 4.